IOPscience iopscience.iop.org

Home Search Collections Journals About Contact us My IOPscience

High-pressure phase transition in $Y_3Fe_5O_{12}$

This content has been downloaded from IOPscience. Please scroll down to see the full text.

2015 J. Phys.: Condens. Matter 27 405401

(http://iopscience.iop.org/0953-8984/27/40/405401)

View the table of contents for this issue, or go to the journal homepage for more

Download details:

IP Address: 128.112.20.228
This content was downloaded on 24/09/2015 at 18:00

Please note that terms and conditions apply.

IOP Publishing Journal of Physics: Condensed Matter

J. Phys.: Condens. Matter **27** (2015) 405401 (10pp) doi:10.1088/0953-8984/27/40/405401

High-pressure phase transition in $Y_3Fe_5O_{12}$

C V Stan[1], J Wang[2], I S Zouboulis[3], V Prakapenka[4] and T S Duffy[2]

[1] Department of Chemistry, Princeton University, Princeton, NJ 08544, USA
[2] Department of Geosciences, Princeton University, Princeton, NJ 08544, USA
[3] Department of Physics, National Technical University of Athens, Athens, Greece
[4] GeoSoilEnviroCARS, University of Chicago, Argonne National Lab, Argonne, IL 60439, USA

E-mail: cstan@princeton.edu

Received 15 July 2015, revised 17 August 2015
Accepted for publication 18 August 2015
Published 24 September 2015

Abstract

Yttrium iron garnet (YIG, $Y_3Fe_5O_{12}$) was examined up to 74 GPa and 1800 K using synchrotron x-ray diffraction in a diamond anvil cell. At room temperature, YIG remained in the garnet phase until abrupt amorphization occurred at 51 GPa, consistent with earlier studies. Upon laser heating up to 1800 K, the material transformed to a single-phase orthorhombic $GdFeO_3$-type perovskite of composition $(Y_{0.75}Fe_{0.25})FeO_3$. No evidence of decomposition of the sample was observed. Both the room-temperature amorphization and high-temperature transformation to the perovskite structure are consistent with the behaviour of other rare earth oxide garnets. The perovskite sample was compressed between 28–74 GPa with annealing to 1450–1650 K every 3–5 GPa. Between 46 and 50 GPa, a 6.8% volume discontinuity was observed without any accompanying change in the number or intensity of diffraction peaks. This is indicative of a high-spin to low-spin electronic transition in Fe^{3+}, likely in the octahedrally coordinated B-site of the perovskite. The volume change of the inferred spin transition is consistent with those observed in other rare earth ferric iron perovskites at high pressures.

Keywords: perovskite, spin transition, x-ray diffraction, rare earth garnet, high pressure

(Some figures may appear in colour only in the online journal)

Introduction

Rare earth garnets have wide application as ferrite, laser, and luminescent materials [1, 2]. The garnet structure of these materials has the general formula $X_3Y_2Z_3O_{12}$ where X, Y, and Z are dodecahedral, octahedral, and tetrahedral sites, respectively. The dodecahedral site is occupied by a rare earth cation while the octahedral and tetrahedral sites are occupied by trivalent Al, Ga, Sc, or Fe. The high-pressure behaviour of compounds in this family has attracted considerable attention. At ambient temperature, pressure-induced amorphization has been observed in various rare earth garnets above 50 GPa including yttrium iron garnet (YIG), $Y_3Fe_5O_{12}$ [3], europium gallium garnet (EGG), $Eu_3Ga_5O_{12}$ [4], gadolinium gallium garnet (GGG), $Gd_3Ga_5O_{12}$ [5, 6], and gadolinium scandium gallium garnet (GSGG), $Gd_3Sc_2Ga_3O_{12}$ [5, 7]. At high pressure–temperature (P–T) conditions, EGG, GGG, and GSGG all transform to the perovskite structure [4, 6, 7]. On the other hand, yttrium aluminum garnet (YAG), $Y_3Al_5O_{12}$, is reported to retain the garnet structure to at least 120 GPa and 700 K [8, 9], although a mechanical instability is predicted theoretically at 108 GPa [10]. The broad stability region for this material has contributed to its utility as an optical pressure sensor in diamond anvil cell experiments [8, 11–14].

High-pressure studies of YIG at ambient temperature have identified several interesting phenomena including pressure-induced amorphization, magnetic collapse, a spin crossover transition, and metallization [3, 15, 16]. X-ray diffraction measurements revealed the occurrence of amorphization above 50 GPa, which was irreversible upon decompression back to ambient pressure [3, 16]. At 48 GPa, Mössbauer spectroscopy indicated that YIG also undergoes a magnetic collapse from a ferrimagnetic to a non-magnetic state at nearly the same pressure as the x-ray amorphization, with the simultaneous disappearance of magnetic moments in both the octahedral and tetrahedral sublattices [15]. The magnetic transition was irreversible down to 1 bar. Abrupt changes in the quadrupole splitting and isomer

 © 2015 IOP Publishing Ltd Printed in the UK

shift were also observed indicating the likely presence of a spin transition accompanying the amorphization [15]. Finally, it was shown that the optical absorption edge vanishes in this pressure range, indicating transition to a metallic state [16]. Thus, YIG garnet simultaneously experiences structural amorphization, magnetic collapse, metallization, and a probable spin transition at 50 GPa.

High pressure-temperature studies of YIG were conducted in the 1960s but were restricted to very low pressures and yield contradictory results. One study reported the decomposition of YIG to $YFeO_3$ and Fe_2O_3 based on examination of samples recovered from compression to 0.4 GPa and 1123 K [17]. Here Fe_2O_3 was in the hematite structure and $YFeO_3$ was an orthorhombic perovskite. However, another study reported the synthesis of a single-phase ferrimagnetic perovskite $(Y_3,Fe)Fe_4O_{12}$ or $(Y_{0.75}Fe_{0.25})FeO_3$ after compressing YIG to 2.52 GPa and 1473 K [18]. A related Mössbauer study demonstrated the existence of two distinct iron sites in the high-pressure YIG phase, supporting the observation of a single-phase perovskite [19]. The differing results obtained in these low-pressure studies have been attributed to different pressure transmitting media and to the fact that reduction of a small fraction of the Fe^{3+} to Fe^{2+} may favor formation of the single perovskite phase over the decomposition reaction [20].

In the present investigation we carried out x-ray diffraction experiments on $Y_3Fe_5O_{12}$ over a wide pressure-temperature range (28–75 GPa, up to 1800 K) using the laser-heated diamond anvil cell (DAC) to determine the phase stability, equation of state, and structural evolution of $Y_3Fe_5O_{12}$ at high pressures.

Methods

A polycrystalline $Y_3Fe_5O_{12}$ sample (Alfa Aesar, 99.9%) was characterized at ambient conditions by x-ray diffraction and Raman spectroscopy. The unit cell parameter was found to be $a = 12.373\,91(3)$ Å, consistent with literature values [18]. High-pressure experiments were carried out with a diamond anvil cell using 200 μm diameter culets. The sample was ground to a few micron grain size and mixed with 10 wt.% gold powder (Goodfellow Corp., 99.95%), which served as a laser absorber and pressure calibrant. Compressed pellets (5–10 μm thick) of this mixture were embedded between layers of NaCl, which acted as a thermal insulator and quasi-hydrostatic pressure medium. Samples were placed within 100 μm diameter holes drilled in Re gaskets that had been pre-indented to 30 μm in thickness.

Angle-dispersive x-ray diffraction was performed at beamline 13-ID-D of the Advanced Photon Source (APS), Argonne National Laboratory. X-rays with a wavelength of 0.3344 Å were directed through the diamond anvils and the diffracted signal was collected with a CCD detector (MarCCD). The detector position and orientation were calibrated using a CeO_2 standard. High temperature experiments were carried out by double-sided laser heating using two diode-pumped single-mode ytterbium fiber lasers ($\lambda = 1064$ μm), each with output power up to 100 W. Beam-shaping optics were used to produce a flat-topped laser profile with a spot size of ~24 μm. Sample temperatures were measured from both sides by spectroradiometry. Details of the x-ray diffraction and laser heating systems at 13-ID-D are reported elsewhere [21]. X-ray diffraction patterns were typically collected for 10–15 s. The resulting 2D CCD images were integrated to produce 1D diffraction patterns using the program FIT2D [22]. Peak positions were determined by fitting background-subtracted Voigt line shapes to the data. Lattice parameters were refined using the program UNITCELL [23] using at least six diffraction lines from each phase observed. The pressure was calculated using the (1 1 1) diffraction peak of gold and its thermal equation of state from [24].

Two separate experiments were performed. In the first, the sample was compressed at room temperature to 51 GPa. The sample was then laser heated at 1550–1700 K for 5–10 min. The sample was further compressed to 74 GPa in ~3 GPa steps and laser heated to 1400–1800 K for 5–10 min at each step. In the second experiment, the sample was compressed to ~30 GPa, and laser heated for 5 min to 1550 K. The synthesized sample was then compressed in 2–4 GPa steps up to 67 GPa with heating for 5 min at 1450–1550 K every 5 GPa.

Results/Discussion

Pressure-induced amorphization

Room-temperature diffraction patterns recorded up to 50.6 GPa consisted of diffraction peaks that could all be assigned either to $Y_3Fe_5O_{12}$ garnet, the NaCl insulator (B1 or B2 phase) or the gold pressure standard (figure 1). The diffraction peaks remained generally sharp but exhibited modest broadening with increasing pressure, likely as a result of increasing differential stress. Upon further increase of pressure from 50.6 to 51.1 GPa, the $Y_3Fe_5O_{12}$ garnet diffraction peaks completely disappeared (figure 1). This indicates that the sample undergoes an abrupt structural transition to a disordered or amorphous state over a narrow pressure range, consistent with previous work [3].

Pressure-induced amorphization (PIA) has also been reported in other rare-earth garnets, including EGG, GGG and GSGG, at 85 GPa, 84(4) GPa, and 62(2) GPa, respectively [4–7]. EGG, GGG and GSGG all transform to a perovskite structure at high pressure-temperature conditions [4, 6, 7]. PIA is commonly observed in framework structures, such as the garnet structure, which can be envisioned as a framework of alternating corner-sharing tetrahedra and octahedra. In EGG, GGG and GSGG, the amorphization has been proposed to be related to instabilities in this corner-sharing network with the increase in pressure [4]. The amorphization pressure has been correlated with the crystal field strength (CFS) of the garnets [5], which has been found empirically to increase as a function of decreasing unit cell size [25]. It has also been proposed that amorphization in these materials is driven by low- or room-temperature kinetic hindrance of a crystalline phase transition [4]. For instance, in YIG, the local atomic structure in the amorphous state was found to be dominated by iron-oxygen FeO_6 complexes with disordered orientation of local axis [3]. Furthermore, all Fe^{3+} ions in the amorphous YIG structure

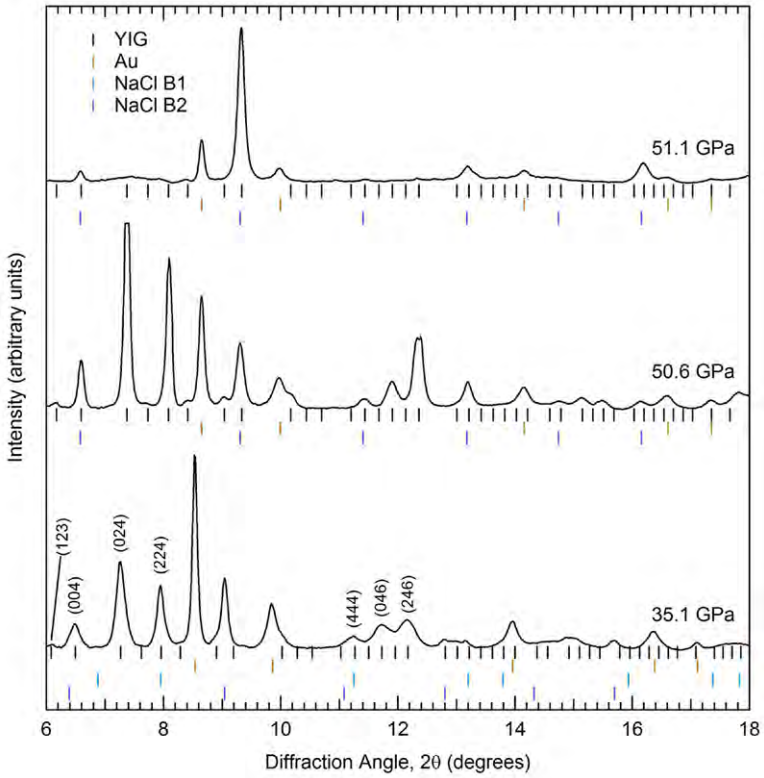

Figure 1. Room-temperature x-ray diffraction patterns of YIG between 35.1 and 51.1 GPa. Calculated peak locations for YIG, Au, and NaCl (in B1 or B2 phase) are shown as ticks below each diffraction pattern. Selected (hkl) values for YIG peaks are indicated.

were found to be octahedrally coordinated [3], which means that the Fe^{3+} from the garnet tetrahedral site must undergo a coordination change. If the kinetically hindered transition involves coordination changes, then the *d* orbitals and their CFS would play a key role in controlling the amount of energy required to undergo the transition, and would act as mediators of the amorphization pressure. In contrast to YIG, the amorphization occurs over a broader pressure range for EGG, GGG and GSGG, with pronounced peak broadening beginning at 75 GPa for EGG, 74(3) GPa for GGG and at 55.5(5) GPa for GSGG. That is, the amorphization occurs over a range of 7–10 GPa in these materials, in contrast to <1 GPa for YIG. The amorphization is irreversible in GGG and GSGG, as the amorphous phase is retained upon decompression to 1 bar [5], while the decompression behaviour of amorphous EGG has not been reported.

Pressure-induced amorphization has received considerable attention and has been reported in a wide range of materials [26–28]. This phenomenon occurs when pressure induces instabilities in the crystal lattice but there is insufficient energy to permit the formation of a more stable crystalline phase, resulting in the loss of long-range order [28]. Two different approaches to understanding this type of amorphization have been proposed, one thermodynamic and one mechanical. In the thermodynamic case, the amorphization phenomenon is similar to melting, but occurs below the crystalline-glass phase transition for the material. In the mechanical case, the structure becomes amorphous when its mechanical stability is violated. The mechanical stability can be tested by examining the Born stability criteria [28]. In the case of a cubic crystal, such as garnet, these can be described by relationships among the elastic constants:

$$C_{11} + 2C_{12} > 0;\ C_{44} > 0;\ C_{11} - C_{12} > 0 \tag{1}$$

The high-pressure elastic constants of YIG can be estimated using the ambient pressure values ($C_{11} = 269$ GPa, $C_{12} = 107.7$ GPa, $C_{44} = 76.4$ GPa [29]), and the measured pressure derivatives of the elastic constants ($\mathrm{d}C_{11}/\mathrm{d}P = 6.22$, $\mathrm{d}C_{12}/\mathrm{d}P = 4.01$, $\mathrm{d}C_{44}/\mathrm{d}P = 0.41$ [30]) through the following relationship [31]:

$$C_{ij} = C_{ij}^{0} + P\left(\frac{\mathrm{d}C_{ij}}{\mathrm{d}P}\right)\left(\frac{V}{V_0}\right)^{\frac{1}{3}} \tag{2}$$

At 50 GPa, all the Born criteria remain satisfied and no elastic softening is observed for YIG and thus there is no evidence for a mechanical instability.

High P–T experiments

At 51 GPa the amorphous sample was heated to 1650 K for 5–10 min. New diffraction peaks quickly appeared after three minutes of heating. The new peaks can be indexed to an orthorhombic unit cell and the peak positions match the $GdFeO_3$-type perovskite phase (space group P*bnm*) (figure 2). All other observed peaks can be identified as either NaCl or Au. No further changes in the diffraction pattern were observed after 30 min of heating at 1375–1775 K or upon quenching to

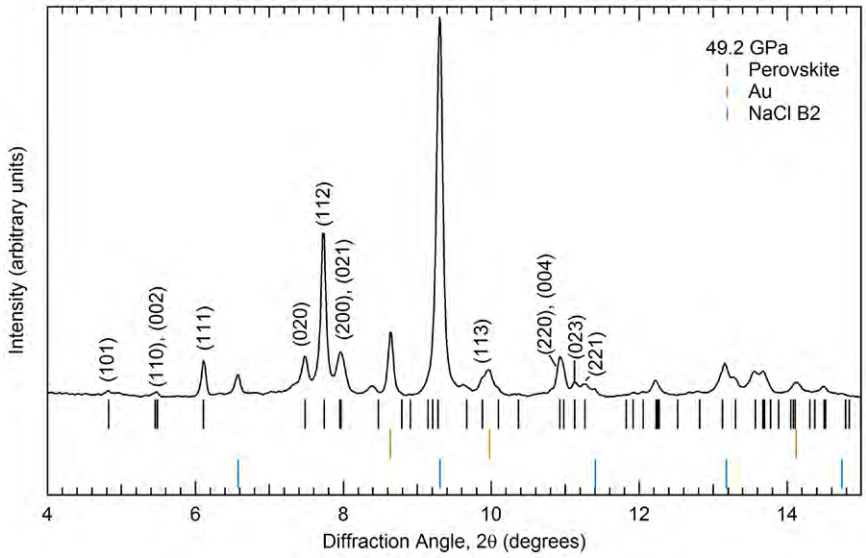

Figure 2. X-ray diffraction pattern of $Y_3Fe_5O_{12}$ at 49.2 GPa, quenched after heating at 1650 K and 51.1 GPa. The pattern can be fit to an orthorhombic unit cell with $a = 4.822(6)$ Å, $b = 5.127(5)$ Å and $c = 6.991(4)$ Å. The tick pattern beneath shows the expected peak locations for P*bnm* perovskite structure (black). Au (yellow) and NaCl (blue) peak locations, as well as Miller indices ($h\,k\,l$) for selected perovskite peaks.

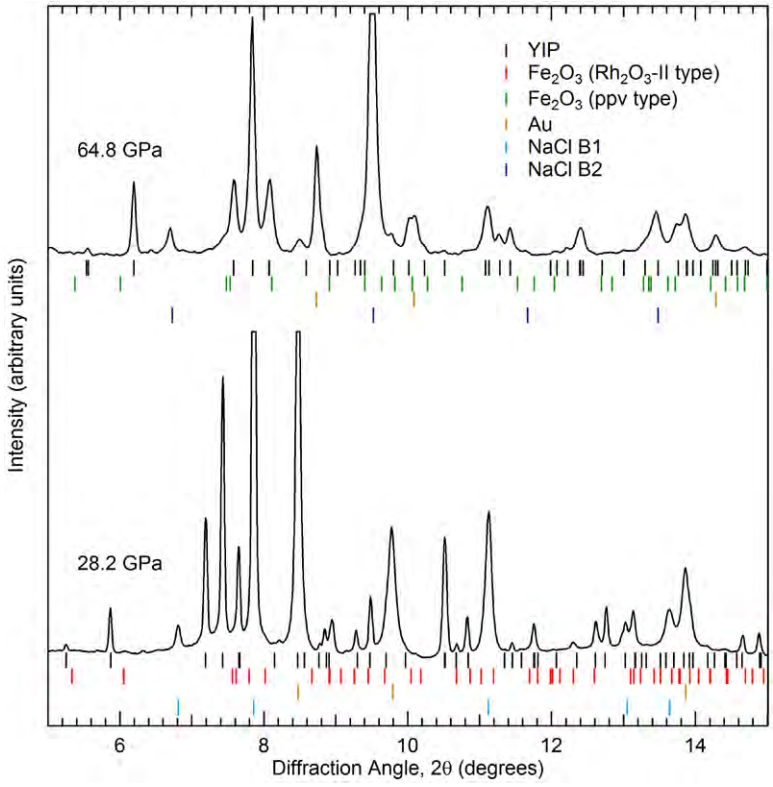

Figure 3. $(Y_{0.75}Fe_{0.25})FeO_3$ perovskite (YIP) diffraction upon quench. At 28.2 GPa, YIP peaks are fit to an orthorhombic P*bnm* unit cell with $a = 5.017(3)$ Å, $b = 5.333(2)$ Å and $c = 7.288(2)$ Å. Tick marks show expected peak locations for other candidate phases including Rh_2O_3-type Fe_2O_3 [38]. At 64.8 GPa, the YIP unit cell is fit with $a = 4.753(4)$ Å, $b = 5.059(3)$ Å, $c = 6.900(4)$ Å. There is no evidence for peaks of $CaIrO_3$-type Fe_2O_3 [36, 37, 39].

room temperature. The pressure measured upon quenching is reduced slightly to 49.2 GPa, likely as a result of relaxation of differential stress. The sample was then further compressed to 74 GPa in 2–3 GPa steps with annealing for 5–10 min to 1550–1650 K at every other step, and the perovskite diffraction peaks continued to be observed up to the highest pressure measured.

A second YIG sample was compressed to 30.7 GPa at room temperature followed by laser heating at 1550 K for 5 min. The YIG peaks disappeared rapidly after heating began, and a new set of diffraction lines appeared. These new peaks can also be indexed as orthorhombic perovskite (figure 3). This indicates that the perovskite phase is stabilized at high temperatures

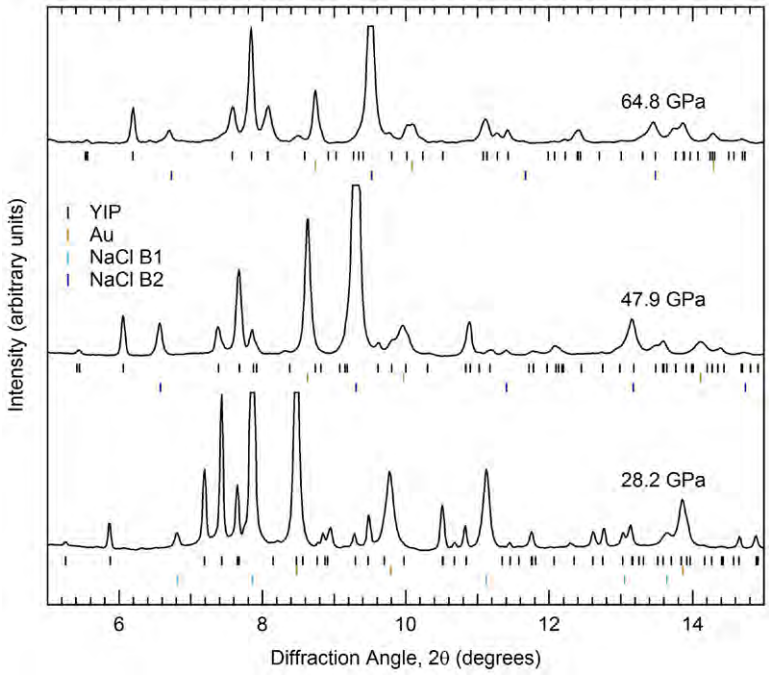

Figure 4. $(Y_{0.75}Fe_{0.25})FeO_3$ perovskite diffraction patterns at selected pressures. All peaks can be indexed as perovskite (YIP), Au or NaCl in the B1 or B2 phase. The *d* spacings corresponding to selected perovskite peaks for each of these diffraction patterns are reported in table 1.

well below the room-temperature amorphization pressure, suggesting that the abrupt amorphization is not simply related to a solid–solid phase boundary. This sample was then further compressed to 64 GPa in 2–3 GPa steps, with annealing every 5 GPa to 1450–1550 K. Again, only peaks from orthorhombic perovskite could be observed over this range.

The orthorhombic ABO_3 perovskite structure consists of 8-fold coordinated A cations located within a framework of octahedrally coordinated B cations. In the case of YIG, two different garnet to perovskite synthesis pathways have been proposed, leading to differences in the A and B site occupancy. YIG could transform into a single-phase perovskite of composition $(Y_{0.75}Fe_{0.25})FeO_3$, where Y^{3+} and Fe^{3+} share the A site in 3 : 1 stoichiometry and Fe^{3+} occupies the B site [18]. Alternatively, YIG could undergo disproportionation into Fe_2O_3 and $YFeO_3$-perovskite, where Y^{3+} alone occupies the A site and Fe^{3+} occupies the B site [17]. At room pressure, Fe^{3+} in 8-fold coordination is expected to have a radius 20% smaller than that of Y^{3+} [32], so the inclusion of Fe^{3+} into the A site would lead to a small reduction in the unit cell volume in $(Y_{0.75}Fe_{0.25})FeO_3$ versus $YFeO_3$, but the diffraction peak positions of $YFeO_3$ and $(Y_{0.75}Fe_{0.25})FeO_3$ would be expected to be similar.

In the case of disproportionation, however, additional peaks associated with Fe_2O_3 would also be present. While there are conflicting reports on the high-pressure phase transition in Fe_2O_3 at room temperature [33–36], previous high-temperatures studies consistently find a phase transition from hematite to an Rh_2O_3(II)-type structure (orthorhombic, P*bcn*) at pressures of above ~25 GPa [33–38]. The Rh_2O_3(II)-type structure contains only one crystallographically distinct cation site and has an x-ray diffraction pattern that is indistinguishable from the orthorhombic P*bnm* perovskite structure. We do not observe evidence of either the hematite or Rh_2O_3(II)-type structures of Fe_2O_3 in our diffraction pattern at 28.2 GPa (figure 3). The expected unit cell parameters for the Fe_2O_3 high-pressure phase at 27 GPa and 300 K are approximately $a = 4.918$ Å, $b = 5.071$ Å, and $c = 7.187$ Å [38]. These are not consistent with the orthorhombic unit cell parameters we measured at 28.2 GPa: $a = 5.017(3)$ Å, $b = 5.333(2)$ Å, $c = 7.288(2)$. The intense (1 1 2) peak ($I/I_0 = 100$) of the Rh_2O_3(II)-type structure, expected to be at $2\theta = 7.61°$, is not observed, nor is there evidence for other low-angle peaks of this structure. Since all observed peaks can be accounted for by a single perovskite-type phase, Au, or NaCl, we conclude that our diffraction patterns are consistent with formation of a single-phase yttrium iron perovskite (YIP) with stoichiometry $(Y_{0.75}Fe_{0.25})FeO_3$. No additional peaks indicative of ordering of Y^{3+} and Fe^{3+} along the A site are present, and thus we conclude the YIP is an A-site disordered perovskite. At higher pressure and temperature conditions ($P > 50$ GPa, $T \sim 2000$ K), Fe_2O_3 is reported to adopt a $CaIrO_3$-type post-perovskite structure (orthorhombic, C*mcm*) [36, 37, 39], although one study reports an alternative orthorhombic high-pressure phase for Fe_2O_3 above 44 GPa [38]. Again, peaks indicating the presence of the post-perovskite phase, particularly the highest intensity (0 2 2) peak at $2\theta = 7.48°$, or those of the alternative orthorhombic high-pressure phase [38] were not observed in our sample, indicating that the sample remains a single-phase perovskite throughout the pressure and temperature range examined in this study (figure 3). Representative diffraction patterns across our pressure range are shown in figure 4, and comparisons of the measured and calculated *d* spacings of YIP at these pressures are recorded in table 1. The garnet to perovskite phase transition is accompanied by a ~8% decrease in volume, ΔV, which is consistent with the ~6–10% ΔV

Table 1. Comparison of observed and calculated d spacings for the perovskite phase of $(Y_{0.75}Fe_{0.25})FeO_3$ at selected pressures.

Pressure (GPa)	h	k	l	d_{obs} (Å)	d_{calc} (Å)	Δd (Å)
28.2 GPa: $a = 5.017(3)$ Å, $b = 5.333(2)$ Å, $c = 7.288(2)$ Å and $V = 195.0(1)$ Å^3						
	1	1	1	3.267 49	3.265 93	0.001 56
	0	2	0	2.666 08	2.665 42	0.000 66
	1	1	2	2.580 85	2.581 20	−0.000 35
	1	1	3	2.022 39	2.024 48	−0.002 09
	2	2	0	1.825 57	1.826 06	−0.000 49
	0	0	4	1.825 57	1.824 30	0.001 27
	0	2	3	1.796 26	1.796 71	−0.000 45
	2	2	1	1.772 23	1.771 44	0.000 79
47.9 GPa: $a = 4.841(6)$ Å, $b = 5.192(4)$ Å, $c = 7.042(6)$ Å and $V = 177.0(2)$ Å^3						
	1	1	1	3.164 59	3.162 24	0.002 35
	0	2	0	2.597 13	2.595 41	0.001 72
	1	1	2	2.499 54	2.496 67	0.002 87
	1	1	3	1.956 11	1.9569	−0.000 79
	2	2	0	1.768 40	1.7693	−0.000 90
	0	0	4	1.762 00	1.761 55	0.000 45
	0	2	3	1.740 35	1.7415	−0.001 15
	2	2	1	1.716 27	1.716 03	0.000 24
64.8 GPa: $a = 4.753(4)$ Å, $b = 5.059(3)$ Å, $c = 6.900(4)$ Å and $V = 165.9(1)$ Å^3						
	1	1	1	3.094 85	3.095 31	−0.000 46
	0	2	0	2.528 36	2.529 89	−0.001 53
	1	1	2	2.445 64	2.443 76	0.001 88
	1	1	3	1.915 10	1.915 39	−0.000 29
	2	2	0	1.731 29	1.731 89	−0.000 60
	0	0	4	1.723 35	1.724 13	−0.000 78
	0	2	3	1.702 39	1.701 36	0.001 03
	2	2	1	1.680 12	1.679 73	0.000 39

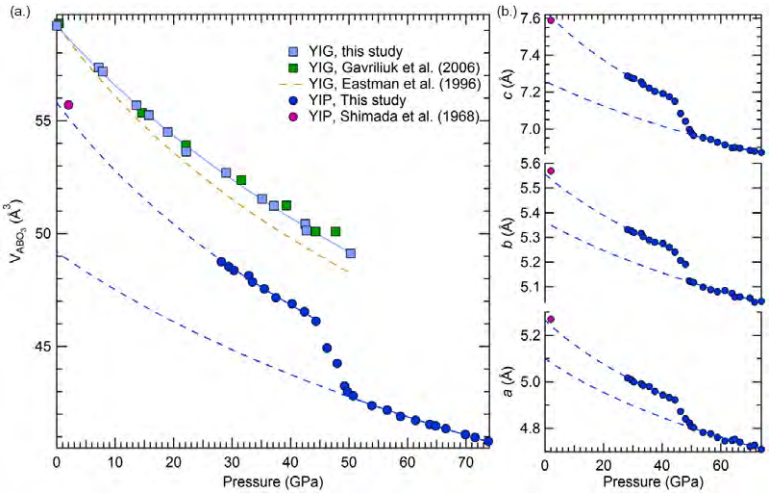

Figure 5. (a) Measured volumes (per ABO_3 unit) of $Y_3Fe_5O_{12}$ garnet and perovskite. The Eastman *et al* [43] equation of state is derived from ultrasonic measurements corrected to isothermal conditions. The Shimada *et al* [18] data point was collected at 2 GPa, and is used in the equation of state fit for the low-pressure data. Equations of state (solid lines) have been extrapolated where shown as dashed lines. (b) Lattice parameters of the perovskite phase as a function of pressure. Colors are the same as those in (a). Equation of state fits are based on the parametric form of the third-order Birch–Murnaghan equation of state [65].

observed in the garnet-perovskite transition in EGG, GSGG, and GGG [4, 6, 7].

Equation of state and spin transition

The unit cell volume of $Y_3Fe_5O_{12}$ garnet was measured up to 51.1 GPa and the results are consistent with those reported by [2] (figure 5(a)). Fitting a third-order Birch–Murnaghan equation of state to the P–V data results in an isothermal bulk modulus, K_{T0}, of 204(5) GPa with pressure derivative $K'_{T0} = 3.1(3)$. V_0 was fixed at to our refined value of 1894.61(1) Å^3. When K'_{T0} is held fixed at 4, a bulk modulus of 189(1) GPa is obtained. These values differ from those reported by ultrasonic elasticity measurements which report

Table 2. Measured unit cell parameters of $(Y_{0.75}Fe_{0.25})FeO_3$ perovskite as a function of pressure.

Pressure (GPa)	*a* (Å)	*b* (Å)	*c* (Å)	*V* (Å^3)
2.0[a]	5.27	5.57	7.59	222.8
28.2	5.017(3)	5.333(2)	7.288(2)	195.0(1)
29.4	5.009(7)	5.327(1)	7.277(1)	194.2(1)
30.3	4.999(6)	5.321(1)	7.274(2)	193.5(1)
32.8	4.992(6)	5.317(4)	7.255(5)	192.6(2)
33.5	4.984(2)	5.303(1)	7.242(2)	191.5(1)
35.5	4.980(4)	5.289(3)	7.222(4)	190.2(1)
37.5	4.959(4)	5.281(3)	7.203(4)	188.7(1)
40.2	4.943(3)	5.276(2)	7.192(3)	187.6(1)
42.4	4.932(5)	5.261(3)	7.175(4)	186.2(2)
44.3	4.923(6)	5.241(4)	7.150(5)	184.5(2)
46.2	4.87 (1)	5.207(7)	7.083(9)	179.7(3)
47.9	4.841(6)	5.192(4)	7.042(6)	177.0(2)
49.7	4.82(2)	5.12(2)	7.01(2)	174.4(7)
50.7	4.803(5)	5.118(3)	6.965(4)	171.2(1)
53.9	4.782(3)	5.099(2)	6.953(3)	169.5(1)
56.5	4.776(1)	5.089(1)	6.942(1)	168.7(1)
58.8	4.761(5)	5.081(3)	6.928(4)	167.6(1)
61.4	4.746(2)	5.086(1)	6.914(2)	166.9(1)
63.8	4.748(5)	5.075(4)	6.898(5)	166.2(2)
64.8	4.753(4)	5.059(3)	6.900(4)	165.9(1)
66.5	4.740(3)	5.060(2)	6.896(3)	165.4(1)
69.9	4.723(2)	5.055(1)	6.885(2)	164.4(1)
71.5	4.727(5)	5.039(4)	6.880(5)	163.9(2)
73.8	4.71(1)	5.042(8)	6.87(1)	163.2(4)

[a] Shimada *et al* [18].

values for the adiabatic bulk modulus, $K_{S0,}$ of 159–163 GPa [29, 40–43]. This difference is likely the result of differential stress during room-temperature compression in an NaCl medium which is known to yield an overestimate of the bulk modulus in the axial diamond anvil cell geometry [44].

Room-temperature equation of state data were obtained for YIP from 28.2–74.0 GPa (table 2). Representative diffraction patterns over this range are shown in figures 2–4. The measured unit cell volumes and individual lattice parameters of YIP are shown as a function of pressure in figure 5. Remarkably, we observe a large (6.8%) reduction in volume between 46 and 50 GPa without the appearance of any new peaks or other changes in the diffraction pattern (figure 4). The same behaviour can also be observed in the individual lattice parameters (figure 5(b)). There is a 2.7%, 2.4% and 2.5% reduction in the *a*, *b*, and *c* lattice parameters over this pressure range, indicating a nearly isotropic volume reduction. These changes are indicative of an isosymmetric phase transition that we attribute to a high-spin to low-spin transition in yttrium iron perovskite as discussed below.

Pressure-induced spin transitions have been reported in a number of Fe-bearing phases in recent years [45–47]. Andradite ($Ca_3Fe_2Si_3O_{12}$), a calcium silicate garnet with Fe^{3+} in the octahedral site, has been reported to undergo a spin transition at 60–70 GPa at room temperature, resulting in a 2.5% volume collapse [46]. Spin transitions have also been observed in a number of perovskites [48–53] and perovskite-related structures [54–57] with Fe^{3+} in octahedral coordination. The Fe^{3+}-bearing rare earth oxide perovskites, $NdFeO_3$, $LaFeO_3$, $PrFeO_3$, $LuFeO_3$ and $EuFeO_3$ were all found to undergo high-spin to low-spin transitions with a volume change of 2.8–6.5% at 30–60 GPa [48–50, 58] (table 3). $NdFeO_3$ was examined using optical spectroscopy and x-ray diffraction, which revealed a volume discontinuity concurrent with an electronic transition that the authors interpreted as being due to a spin transition in Fe^{3+} [58]. $LuFeO_3$, $LaFeO_3$, $PrFeO_3$ and $EuFeO_3$ were studied by high-pressure x-ray diffraction, Raman spectroscopy, and Mössbauer spectroscopy, and a volume discontinuity was observed for all four. This was concurrent with a transition to a paramagnetic state and a significant change in the quadrupole splitting in the Mössbauer spectra, indicative of a spin transition in all of these compounds as well [48–50, 59]. The percentage volume change across the spin transition in these perovskites is inversely correlated to the ionic radius of the rare earth cation in the 8-fold A site (figure 6). This largely reflects the relative sizes of the A and B sites: the relative volume collapse in the octahedral B site is larger when the A site is smaller. Thus YIP, for which the A site is occupied by yttrium with a relatively small radius (and Fe^{3+}), exhibits a relatively large volume change, as expected from this trend.

Equations of state were fit to YIP both above and below the spin transition using the third-order Birch–Murnaghan equation (figure 5(a)). K'_{T0} was fixed to 4.0 in both cases. The high-spin phase can be fit with $V_0 = 223(1)$ Å^3 and $K_{T0} = 161(9)$ GPa using data from this study only, or $V_0 = 225.2(8)$ Å^3 and $K_{T0} = 150(4)$ GPa when including a low-pressure datum from [18]. For the low-spin phase, we obtain $V_0 = 197(1)$ Å^3 and $K_{T0} = 272(11)$ GPa. These results are preliminary, as the volumes have been constrained over only limited ranges of compression. Nevertheless, the results suggest that the compressibility of the high-spin perovskite phase is similar to that of the garnet phase (based on ultrasonic elasticity data) but that there is a large decrease in compressibility across the spin transition. This is broadly consistent with static compression results for other rare earth ferric iron perovskites which may exhibit as much as a 30–40% increase in bulk modulus across the spin transition (table 3).

In $(Y_{0.75}Fe_{0.25})FeO_3$, iron occupies 100% of the B sites as well as a 25% of the A sites. Thus, a spin transition could occur in either or both sites. While additional studies such as Mössbauer spectroscopy are necessary to address this question, insight can be obtained from consideration of the high-pressure spin transition in Fe-bearing silicate perovskites. In the case of (Mg, Fe)(Al, Si, Fe)O_3, the behaviour of Fe cations depends on site occupancy and valence [45, 60–62]. For ferric iron, both theoretical calculations and experiments indicate that Fe^{3+} in the A site remains in the high spin state until pressures above 100 GPa, whereas Fe^{3+} in the B site undergoes a pressure-induced spin transition at ~20–70 GPa [60, 62–64]. This is likely related to the longer Fe–O distances in the more highly coordinated A site. The almost spherical ligand field of the high-spin state of the A-site Fe^{3+} ion is caused by the full occupancy of its 3*d* orbitals, having the 3D representation e_g. It appears that this charge distribution maintains its spherical symmetry in the pressure range of this experiment. By

Table 3. Comparison of properties for rare earth orthoferrite perovskites ($AFeO_3$).

Reference	Composition	High spin		Low spin		ΔP	ΔV	A^{3+} cation
		V_0 (Å^3)	K_{T0} (GPa)	V_0 (Å^3)	K_{T0} (GPa)	(GPa)	(%)	radius (Å)
This study	$(Y_{0.75}Fe_{0.25})FeO_3$	223(1)	161(9)	197(1)	272(11)	46–50	6.8	0.959
Rozenberg *et al* [48]	$LuFeO_3$	218.4(4)	241(5)	199.4(9)	313(10)	47–58	6.5	0.977
	$EuFeO_3$	230.7(2)	241(2.5)	214.4(6)	339(7)	46–51	4.7	1.066
	$PrFeO_3$	239.3(3)	274(5)	218.6(1.2)	312(7)	33–58	4.0	1.126
Xu *et al* [49]	$PrFeO_3$					35–50	2.8	1.126
	$LaFeO_3$					35–50	3.0	1.160
Gavriliuk *et al* [58]	$NdFeO_3$		244(4)		239(4)	35–42	4.0	1.109

A^{3+} cation radius is from [32]. In the case of YIP, the value has been calculated based on the radii of Y^{3+} (1.019 Å) and (high spin) Fe^{3+} (0.78 Å).
V_0: zero-pressure volume.
K_{T0}: isothermal bulk modulus.
ΔP: pressure range of high spin to low spin transition.
ΔV: change in volume across the transition.

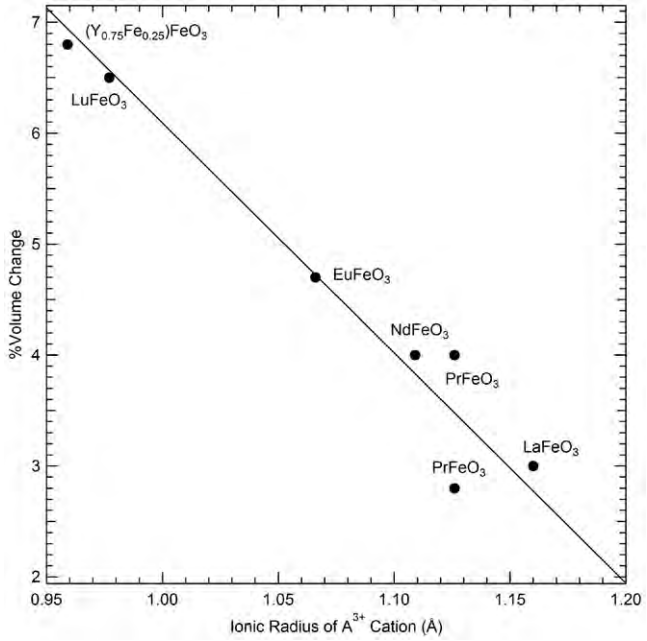

Figure 6. Percentage volume discontinuity in rare earth perovskites across the spin transition as a function of A cation radius. Ionic radii are taken from [32]. Measured volume discontinuities are from this work and [48, 58, 59]. For YIP, the mean ionic radius is determined from the proportions of Y^{3+} and Fe^{3+} in the A site, i.e. in 3 : 1 stoichiometry. The solid line shows the linear fit to the data.

contrast, the octahedral coordination of the Fe^{3+} ions occupying the B-sites leads to a 3D representation t_{2g} of the corresponding orbitals. These orbitals direct themselves away from the 6 O^{2-} ions linked to each B-site Fe^{3+} ion. This orientation favors the pressure-dependent shortening the Fe–O bonds in the FeO_6 octahedra [47]. Thus, by analogy with silicate perovskite, we expect the spin transition is occurring in the B site while the fraction of Fe^{3+} in the A site likely remains high spin. This is supported by the magnitude of the volume change of the transition which is consistent with the trend in other rare earth perovskites with Fe^{3+} confined only to the B site (figure 6).

This pressure-instigated breakdown of Hund's rule of maximum spin forces energetically lower orbitals to become occupied by a pair of electrons of opposite spin, leading to a downsizing of the whole crystal structure without any symmetry change. The pressure-actuated close-packing arrangement should also take into account the orientation and occupancy of the valence electron orbitals at the relevant crystal structure sites. Thus pressure is a powerful tool for the controlled alteration of the physical and chemical properties of materials. Be it subtle, gradual, or abrupt (phase-transitional), pressure variation affects the short- as well as the long-range behaviour of atoms or ions constituting or embedded in the structure under investigation. The high-pressure high-to-low-spin phase transition of YIP described above is a manifestation of the application of quantum mechanical principles, or, more accurately, of the pressure-mediated breach of these principles, in the macroscopic scale.

Conclusion

Static compression experiments were performed in the laser-heated diamond anvil cell on yttrium iron garnet ($Y_3Fe_5O_{12}$, YIG) to a maximum pressure of 74 GPa and temperature of ~1800 K. At room temperature, we confirmed the sudden onset of amorphization in YIG near 51 GPa. Upon laser heating of either the garnet structure at 28 GPa or pressure-amorphized material at 51 GPa, $Y_3Fe_5O_{12}$ transforms into an orthorhombic perovskite structure ($GdFeO_3$-type). Due to the absence of diffraction peaks that would indicate the presence of iron oxide (Fe_2O_3), the composition of the synthesized perovskite (YIP) was inferred to be $(Y_{0.75}Fe_{0.25})FeO_3$, in agreement with other low-pressure studies [18, 19]. The room-temperature equation of state of yttrium iron perovskite was measured from 28 to 74 GPa. The sample was observed to undergo an isosymmetric volume change of 6.8% between 46 GPa and 50 GPa. The persistence of the YIP peaks and the pressure range and volume change of the discontinuity are consistent with a high-spin to low-spin transition in Fe^{3+} in the B site of yttrium iron perovskite. Our results are consistent with the observed behaviour of spin transitions in other ferric iron-containing perovskites with Fe^{3+} occupying the octahedral B site [47]. Additional studies, such as x-ray emission spectroscopy and Mössbauer spectroscopy, are needed to further characterize the high-pressure transition in this material.

Acknowledgments

We benefitted from discussions with Gregory Finkelstein, June Wicks and Earl O'Bannon. This work was supported by the National Science Foundation (NSF) and the Carnegie-DOE Alliance Center. The experiments were performed at GeoSoilEnviroCARS of the Advanced Photon Source, Argonne National Laboratory. Use of the APS, an Office of Science User Facility, was supported by the U.S. Department of Energy (DOE) under Contract No. DE-AC02-06CH11357. GeoSoilEnviroCARS (Sector 13) is supported by the NSF—Earth Sciences (EAR-1128799), and the DOE, Geosciences (DE-FG02-94ER14466). I S Z acknowledges support from the National Technical University of Athens during his sabbatical stay at Princeton University.

References

[1] Adam J D, Davis L E, Dionne G F, Schloemann E F and Stitzer S N 2002 Ferrite devices and materials *IEEE Trans. Microw. Theory Tech.* **50** 721–37
[2] Geusic J E, Marcos H M and Uitert L G V 1964 Laser oscillations in Nd-doped yttrium aluminum, yttrium gallium and gadolinium garnets *Appl. Phys. Lett.* **4** 182–4
[3] Gavriliuk A G, Struzhkin V V, Lyubutin I S, Eremets M I, Trojan I A and Artemov V V 2006 Equation of state and high-pressure irreversible amorphization in $Y_3Fe_5O_{12}$ *J. Exp. Theor. Phys. Lett.* **83** 37–41
[4] Lin C L, Li Y C, Li X D, Li R, Lin J F and Liu J 2013 Pressure-induced structural evolution and amorphization in $Eu_3Ga_5O_{12}$ *J. Appl. Phys.* **114** 163521
[5] Hua H, Mirov S and Vohra Y K 1996 High-pressure and high-temperature studies on oxide garnets *Phys. Rev.* B **54** 6200–9
[6] Mao Z, Dorfman S M, Shieh S R, Lin J F, Prakapenka V B, Meng Y and Duffy T S 2011 Equation of state of a high-pressure phase of $Gd_3Ga_5O_{12}$ *Phys. Rev.* B **83** 054114
[7] Lin C, Liu J, Lin J-F, Li X, Li Y, Zhang Q, Xiong L and Li R 2013 Garnet-to-perovskite transition in $Gd_3Sc_2Ga_3O_{12}$ at high pressure and high temperature *Inorg. Chem.* **52** 431–4
[8] Wei Q, Dubrovinskaia N and Dubrovinsky L 2011 Ruby and Sm:YAG fluorescence pressure gauges up to 120 GPa and 700 K *J. Appl. Phys.* **110** 043513
[9] Liu J and Vohra Y K 1996 Photoluminescence and x-ray-diffraction studies on Sm-doped yttrium aluminum garnet to ultrahigh pressures of 338 GPa *J. Appl. Phys.* **79** 7978–82
[10] Goel P, Mittal R, Choudhury N and Chaplot S L 2010 Lattice dynamics and Born instability in yttrium aluminum garnet, $Y_3Al_5O_{12}$ *J. Phys. Condens. Matter* **22** 065401
[11] Hess N J and Schiferl D 1990 Pressure and temperature dependence of laser-induced fluorescence of Sm:YAG to 100 kbar and 700 °C and an empirical model *J. Appl. Phys.* **68** 1953–60
[12] Yusa H, Yagi T and Arashi H 1994 Pressure dependence of Sm:YAG fluorescence to 50 GPa: a new calibration as a high pressure scale *J. Appl. Phys.* **75** 1463–6
[13] Datchi F, Dewaele A, Loubeyre P, Letoullec R, Godec Y L and Canny B 2007 Optical pressure sensors for high-pressure–high-temperature studies in a diamond anvil cell *High Press. Res.* **27** 447–63
[14] Trots D M, Kurnosov A, Boffa Ballaran T, Tkachev S, Zhuravlev K, Prakapenka V, Berkowski M and Frost D J 2013 The Sm:YAG primary fluorescence pressure scale *J. Geophys. Res. Solid Earth* **118** 5805–13
[15] Lyubutin I S, Gavriliuk A G, Trojan I A and Sadykov R A 2005 Magnetic collapse in yttrium iron garnet $Y_3Fe_5O_{12}$ at high pressure *J. Exp. Theor. Phys. Lett.* **82** 702–7
[16] Gavriliuk A G, Struzhkin V V, Lyubutin I S and Trojan I A 2005 Irreversible electronic transition with possible metallization in $Y_3Fe_5O_{12}$ at high pressure *J. Exp. Theor. Phys. Lett.* **82** 603–8
[17] Marezio M, Remeika J P and Jayaraman A 1966 High-pressure decomposition of synthetic garnets *J. Chem. Phys.* **45** 1821–4
[18] Shimada M, Kume S and Koizumi M 1968 Possible existence of dense ferrimagnetic perovskite allotropic form of yttrium iron garnet *J. Am. Ceram. Soc.* **51** 713–5
[19] Shimada M 1971 Mössbauer study of high pressure phase of YIG *Phys. Lett.* **37A** 341–2
[20] Shimada M 1971 Transformation of yttrium iron garnet under pressure *Sci. Rep. Coll. Gen. Educ. Osaka Univ.* **20** 45–58
[21] Prakapenka V B, Kubo A, Kuznetsov A, Laskin A, Shkurikhin O, Dera P, Rivers M L and Sutton S R 2008 Advanced flat top laser heating system for high pressure research at GSECARS: application to the melting behavior of germanium *High Press. Res.* **28** 225–35
[22] Hammersley A P, Svensson S O, Hanfland M, Fitch A N and Hausermann D 1996 2D detector software: from real detector to idealised image or two-theta scan *High Press. Res.* **14** 235–48
[23] Holland T J B and Redfern S A T 1997 Unit cell refinement from powder diffraction data; the use of regression diagnostics *Mineral. Mag.* **61** 65–77
[24] Fei Y, Ricolleau A, Frank M, Mibe K, Shen G and Prakapenka V 2007 Toward an internally consistent pressure scale *Proc. Natl Acad. Sci.* **104** 9182–6
[25] Gruber J B, Hills M E, Morrison C A, Turner G A and Kokta M R 1988 Absorption spectra and energy levels of Gd^{3+}, Nd^{3+}, and Cr^{3+} in the garnet $Gd_3Sc_2Ga_3O_{12}$ *Phys. Rev.* B **37** 8564–74
[26] Sharma S M and Sikka S K 1996 Pressure induced amorphization of materials *Prog. Mater. Sci.* **40** 1–77
[27] Richet P and Gillet P 1997 Pressure-induced amorphization of minerals; a review *Eur. J. Mineral.* **9** 907–33
[28] Machon D, Meersman F, Wilding M C, Wilson M and McMillan P F 2014 Pressure-induced amorphization and polyamorphism: inorganic and biochemical systems *Prog. Mater. Sci.* **61** 216–82
[29] Clark A E and Strakna R E 1961 Elastic constants of single-crystal YIG *J. Appl. Phys.* **32** 1172–3
[30] Yogurtcu Y K, Miller A J and Saunders G A 1980 Elastic behaviour of YAG under pressure *J. Phys. C: Solid State Phys.* **13** 6585–97
[31] Guinan M and Steinberg D 1975 A simple approach to extrapolating measured polycrystalline shear moduli to very high pressure *J. Phys. Chem. Solids* **36** 829
[32] Shannon R D 1976 Revised effective ionic radii and systematic studies of interatomic distances in halides and chalcogenides *Acta Crystallogr.* A **32** 751–67
[33] Pasternak M P, Rozenberg G K, Machavariani G Y, Naaman O, Taylor R D and Jeanloz R 1999 Breakdown of the Mott–Hubbard state in Fe_2O_3: a first-order insulator–metal transition with collapse of magnetism at 50 GPa *Phys. Rev. Lett.* **82** 4663–6
[34] Rozenberg G K, Dubrovinsky L S, Pasternak M P, Naaman O, Le Bihan T and Ahuja R 2002 High-pressure structural studies of hematite Fe_2O_3 *Phys. Rev.* B **65** 064112
[35] Liu H, Caldwell W A, Benedetti L R, Panero W and Jeanloz R 2003 Static compression of α-Fe_2O_3: linear incompressibility of lattice parameters and high-pressure transformations *Phys. Chem. Miner.* **30** 582–8
[36] Bykova E, Bykov M, Prakapenka V, Konôpková Z, Liermann H-P, Dubrovinskaia N and Dubrovinsky L 2013

Novel high pressure monoclinic Fe_2O_3 polymorph revealed by single-crystal synchrotron x-ray diffraction studies *High Press. Res.* **33** 534–45
[37] Ono S, Kikegawa T and Ohishi Y 2004 High-pressure phase transition of hematite, Fe_2O_3 *J. Phys. Chem. Solids* **65** 1527–30
[38] Ito E *et al* 2009 Determination of high-pressure phase equilibria of Fe_2O_3 using the Kawai-type apparatus equipped with sintered diamond anvils *Am. Mineral.* **94** 205–9
[39] Shim S-H, Bengtson A, Morgan D, Sturhahn W, Catalli K, Zhao J, Lerche M and Prakapenka V 2009 Electronic and magnetic structures of the postperovskite-type Fe_2O_3 and implications for planetary magnetic records and deep interiors *Proc. Natl Acad. Sci.* **106** 5508–12
[40] Bateman T B 1966 Elastic moduli of single-crystal europium iron garnet and yttrium iron garnet *J. Appl. Phys.* **37** 2194–5
[41] Haussühl S, Mateika D and Tolksdorf W 1976 Elastische und thermoelastische Konstanten von $Y_3Fe_5O_{12}$-, $Nd_3Ga_5O_{12}$- und $Sm_3Ga_5O_{12}$-Granaten *Z. Nat.—J. Phys. Sci.* **31A** 390–2
[42] Sharma P U and Modi K B 2010 Effect of Fe^{3+} substitution on elastic properties of yttrium iron garnet *Phys. Scr.* **81** 015601
[43] Eastman D E 1966 Measurement of third-order elastic moduli of yttrium iron garnet *J. Appl. Phys.* **37** 2312–6
[44] Duffy T S, Shen G, Heinz D L, Shu J, Ma Y, Mao H-K, Hemley R J and Singh A K 1999 Lattice strains in gold and rhenium under nonhydrostatic compression to 37 GPa *Phys. Rev.* B **60** 15063–73
[45] Badro J 2014 Spin transitions in mantle minerals *Annu. Rev. Earth Planet. Sci.* **42** 231–48
[46] Friedrich A, Winkler B, Morgenroth W, Ruiz-Fuertes J, Koch-Müller M, Rhede D and Milman V 2014 Pressure-induced spin collapse of octahedrally coordinated Fe^{3+} in $Ca_3Fe_2[SiO_4]_3$ from experiment and theory *Phys. Rev.* B **90** 094105
[47] Lin J-F, Speziale S, Mao Z and Marquardt H 2013 Effects of the electronic spin transitions of iron in lower mantle minerals: implications for deep mantle geophysics and geochemistry *Rev. Geophys.* **51** 244–75
[48] Rozenberg G K, Pasternak M P, Xu W M, Dubrovinsky L S, Carlson S and Taylor R D 2005 Consequences of pressure-instigated spin crossover in $RFeO_3$ perovskites; a volume collapse with no symmetry modification *Europhys. Lett.* **71** 228–34
[49] Xu W M, Naaman O, Rozenberg G K, Pasternak M P and Taylor R D 2001 Pressure-induced breakdown of a correlated system: the progressive collapse of the Mott–Hubbard state in $RFeO_3$ *Phys. Rev.* B **64** 094411
[50] Hearne G R, Pasternak M P, Taylor R D and Lacorre P 1995 Electronic structure and magnetic properties of $LaFeO_3$ at high pressure *Phys. Rev.* B **51** 11495–500
[51] Takano M, Nasu S, Abe T, Yamamoto K, Endo S, Takeda Y and Goodenough J B 1991 Pressure-induced high-spin to low-spin transition in $CaFeO_3$ *Phys. Rev. Lett.* **67** 3267–70
[52] Badro J, Rueff J-P, Vankó G, Monaco G, Fiquet G and Guyot F 2004 Electronic transitions in perovskite: possible nonconvecting layers in the lower mantle *Science* **305** 383–6
[53] Badro J, Fiquet G, Guyot F, Rueff J-P, Struzhkin V V, Vankó G and Monaco G 2003 Iron partitioning in Earth's mantle: toward a deep lower mantle discontinuity *Science* **300** 789–91
[54] Pasternak M P, Taylor R D, Jeanloz R, Li X, Nguyen J H and McCammon C A 1997 High pressure collapse of magnetism in $Fe_{0.94}O$: Mössbauer spectroscopy beyond 100 GPa *Phys. Rev. Lett.* **79** 5046–9
[55] Gleason A E, Quiroga C E, Suzuki A, Pentcheva R and Mao W L 2013 Symmetrization driven spin transition in ε-FeOOH at high pressure *Earth Planet. Sci. Lett.* **379** 49–55
[56] Lyubutin I S and Gavriliuk A G 2009 Research on phase transformations in 3d-metal oxides at high and ultrahigh pressure: state of the art *Phys.-Usp.* **52** 989–1017
[57] Gavriliuk A G, Struzhkin V V, Lyubutin I S and Troyan I A 2007 Equation of state and structural transition at high hydrostatic pressures in the $BiFeO_3$ crystal *JETP Lett.* **86** 197–201
[58] Gavriliuk A G, Troyan I A, Boehler R, Eremets M I, Lyubutin I S and Serebryanaya N R 2003 Electronic and structural transitions in $NdFeO_3$ orthoferrite under high pressures *J. Exp. Theor. Phys. Lett.* **77** 619–24
[59] Xu W M, Pasternak M P, Rozenberg G Kh and Taylor R D 2002 Pressure-induced spin-crossover in $EuFeO_3$ *Hyperfine Interact.* **141–142** 243–7
[60] Catalli K, Shim S-H, Prakapenka V B, Zhao J, Sturhahn W, Chow P, Xiao Y, Liu H, Cynn H and Evans W J 2010 Spin state of ferric iron in $MgSiO_3$ perovskite and its effect on elastic properties *Earth Planet. Sci. Lett.* **289** 68–75
[61] Lin J-F, Alp E E, Mao Z, Inoue T, McCammon C, Xiao Y, Chow P and Zhao J 2012 Electronic spin states of ferric and ferrous iron in the lower-mantle silicate perovskite *Am. Mineral.* **97** 592–7
[62] Hsu H, Blaha P, Cococcioni M and Wentzcovitch R M 2011 Spin-state crossover and hyperfine interactions of ferric iron in $MgSiO_3$ perovskite *Phys. Rev. Lett.* **106** 118501
[63] Potapkin V *et al* 2013 Effect of iron oxidation state on the electrical conductivity of the Earth's lower mantle *Nat. Commun.* **4** 1427
[64] Fujino K *et al* 2012 Spin transition of ferric iron in Al-bearing Mg–perovskite up to 200 GPa and its implication for the lower mantle *Earth Planet. Sci. Lett.* **317–318** 407–12
[65] Xia X, Weidner D J and Zhao H 1998 Equation of state of brucite; single-crystal Brillouin spectroscopy study and polycrystalline pressure-volume-temperature measurement *Am. Mineral.* **83** 68–74